1 Context-aware Electromagnetic Design for Continuously Wearable Biosymbiotic Devices

- 2 Authors
- 3 Tucker Stuart^{1,†}, Xiaoyang Yin^{2,†}, Shengjian Jammy Chen^{2,3}, Max Farley¹, Dylan Thomas
- 4 McGuire¹, Nikhil Reddy⁴, Ryan Thien¹, Sam DiMatteo¹, Christophe Fumeaux^{2,*}, Philipp
- 5 Gutruf^{1,5,6,7,*}

6 Affiliations

- ¹Department of Biomedical Engineering, University of Arizona, Tucson, AZ, 85721, USA,
- 8 ²School of Electrical and Electronic Engineering, The University of Adelaide, Adelaide, SA
- 9 5005, Australia.
- ³College of Science and Engineering, Flinders University, Tonsley, SA 5042, Australia.
- ⁴Eller College of Management, University of Arizona, Tucson, AZ 85721, USA.
- ⁵Department of Electrical and Computer Engineering, University of Arizona, Tucson, AZ,
- 13 85721, USA
- ⁶Bio Institute, University of Arizona, Tucson, AZ, 85721, USA
- ⁷Neroscience GIDP, University of Arizona, Tucson, AZ, 85721, USA
- †Contributed equally to this work
- *Corresponding authors: christophe.fumeaux@adelaide.edu.au, pgutruf@arizona.edu.

18 Abstract

19

20

21

22

23

24

25

26

27

28

29

30

31

Imperceptible wireless wearable devices are critical to advance digital medicine with the goal to capture clinical-grade biosignals continuously. Design of these systems is complex because of unique interdependent electromagnetic, mechanic and system level considerations that directly influence performance. Typically, approaches consider body location, related mechanical loads and desired sensing capabilities, however, design for real world application context is not formulated. Wireless power casting eliminates user interaction and the need to recharge batteries, however implementation is challenging because the use case influences performance. To facilitate a data-driven approach to design we demonstrate a method for personalized, context-aware antenna, rectifier and wireless electronics design that considers human behavioral patterns and physiology to optimize electromagnetic and mechanical features for best performance across an average day of the target user group. Implementation of these methods result in devices that enable continuous recording of high-fidelity biosignals over weeks without the need for human interaction.

32

33

34

35

36

37

38

39

40

41

42

43

44

45

46

47

48

49

50

51

52

53

54

55

56

57

58

59

60

61

62

Keywords

Behavior, Electromagnetics, Wireless, Battery-free, Sensors, Wearables

Introduction

Progression towards digital medicine such as early automated diagnostics, personalized therapeutics, and individualized disease management are key developments that promise to modernize the way we diagnose and treat patients. However, progression is slow due to limitations in current wearable device systems (Heikenfeld et al., 2018; T. R. Ray et al., 2019; Stuart et al., 2022, 2021). Conventional wearable devices exhibit several unfavorable characteristics, including poor data reliability (Cho et al., 2021), frequent user interaction (Mercer et al., 2016), and batteryrecharging requirements (Kekade et al., 2018), which prohibit device application with clinically relevant fidelity and fail to promote long-term user engagement needed for realization of the digital medicine concept (Stuart et al., 2022). Key to active disease prevention and treatment at home are wearables that enable continuous, 24/7 clinical data streams with unobtrusive hardware that is accepted by users, even in absence of immediate health issue (Fensli et al., 2008; Spagnolli et al., 2015; Yin et al., 2022). Development of wearable devices aimed at addressing these shortcomings have focused on implementation of soft mechanical structures (Rogers et al., 2010; Dang et al., 2020; Lim et al., 2020; T. Ray et al., 2019; Sunwoo et al., 2021) and wireless power transfer (WPT) (Shadid and Noghanian, 2018; Stuart et al., 2022, 2021), as well as energy harvesting from motion, heat and biofluids (Choi et al., 2017; Nozariasbmarz et al., 2020; Stuart et al., 2022, 2021; Xu et al., 2021; Zou et al., 2021) to provide skin like mechanics and eliminate the need for bulky battery supplies and user interaction, respectively (Kim et al., 2017, 2015; Krishnan et al., 2018; Rahman et al., 2022; Stuart et al., 2021). Among these device-powering modalities, magnetic resonance coupling (MRC) is the most popular in use for wearable devices due to its established infrastructure, high power transfer efficiency and compatibility with established near-field communication protocols and enabled devices (Stuart et al., 2021; Yu et al., 2019). However, operational constraints of MRC limit device function to sedentary or noncontinuous scenarios. More recently, implementation of far-field power casting has been demonstrated as a viable approach with introduction of soft materials schemes leveraging extended operational ranges of up to 2 meters (Huang et al., 2016; Stuart et al., 2021). Despite its extended functional range, adoption of far-field power casting has been hindered due to poor efficiency resulting from large

casting volumes (Xia and Aissa, 2015; Yedavalli et al., 2017), interference with surrounding materials (Dobkin, 2012), and spatial alignment requirements of the antenna structures (Huang et al., 2016). Methods such as beam-steering (Eid et al., 2021; Lee et al., 2019; Shuai et al., 2021) and deployment of antenna arrays (Sun et al., 2008; Tong and Geyi, 2016) have aimed to address these hurdles, but are limited in application due to cost, energy consumption, and large volume occupied by casting infrastructure.

To enable wearable devices that are almost imperceptible and deliver clinical-grade biosignals continuously without user burden, schemes to enable far-field power casting are critical. In current electromagnetic designs, environmental factors, distance to power casting units, worn antenna gain radiation pattern, and physiological characteristics of the intended wearer are considered. However, a critical parameter that is often neglected is human behavior and variance thereof, because information has been traditionally hard to quantify. Specifically, for far-field power casting systems, precise and statistically relevant characterization of the application scenario and full system optimization are critical to enable next generation wearables. Recent

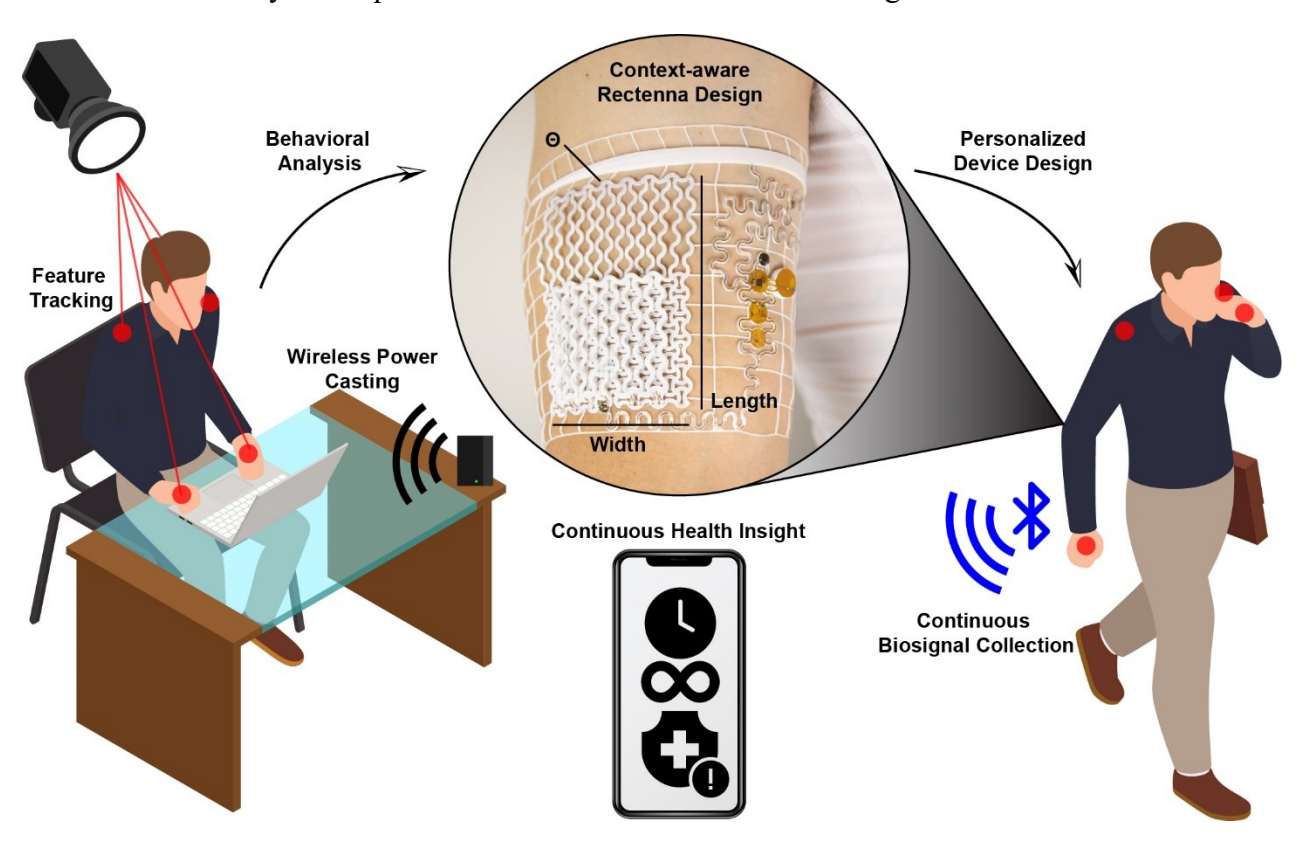


Fig. 1 Behaviorally Driven Antenna Design for Continuously Wearable Biosymbiotic Devices: Schematically illustrated working principle showing behavioral pattern identification and subsequent antenna design for collection of uninterrupted, high-fidelity data streams.

developments in automated behavioral analysis based on neural nets paired with advances in 3D printed wearable device creation allow for highly personalized and application-specific designs that are completely digitally designed and manufactured. This emerging design paradigm enables data-driven and highly optimized solutions for several applications.

Materials and Methods

77

78

79

80

81

82

83

84

85

86

87

88

89

90

91

92

93

94

95

96

97

98

99

100

101

102

103

104

105

Detailed descriptions of the methods and system used in these experiments can be found in the Methods section. This includes information on device fabrication and characterization, behavioral data collection and analysis, mechanical and electromagnetic finite element analysis, and long-term experimental procedures.

Results and Discussion

Data-Driven and Context-aware Digital Rectenna and System Design

In this work we introduce the concept to utilize behavioral analysis for optimized antenna and rectifier designs. This approach facilitates optimized wireless powering solutions with tailored mechanics to realize personalized wearables for the indefinite collection of high-fidelity biosignals (Fig. 1). To achieve this, we employ deep neural net analysis of a cohort of subjects in application scenarios, such as office work with an active lifestyle, which can be analyzed to extract characteristic parameters such as orientation, distance, angular offset, and relative spatial location to the power casting devices with statistical significance. These parameters are critical in determining electromagnetic characteristics of antennas and rectifiers to create context-aware designs that tune key parameters, such as impedance of these components to achieve optimum system performance. This information, paired with digital manufacturing techniques (Stuart et al., 2021), enables creation of personalized rectennas that are realized through fusion deposition modeling (FDM) printing according to the specifications obtained from behavioral observations. This concept improves far-field power casting for wearable sensing devices, allowing robust device operation without the need for large energy storage or restrictions to user mobility. The system design process enables deployment of wearable sensor systems that can collect uninterrupted steams of high-fidelity biosignals over multiple weeks without the need for user interaction. This can be achieved through powering using consistent wireless energy influx, which theoretically enables years of use without user hardware interaction.

Human Behavioral Studies

Human behavioral patterns can be exploited in rectenna (rectifier and antenna) design to optimize average power casting efficiency by tailoring to most statistically relevant scenarios of use. Deep neural net enabled video analysis typically used in neuroscience research (Wei and Kording, 2018) can be employed to capture a large majority of the modern workforce behavior, which includes prolonged hours of desk work, offering settings with potential to cast energy to power wearable sensing devices. The process to acquire behavior from a cohort of test subjects (n=10) is described schematically in Fig. 2A and begins with video collection of subject activity. Relevant physiological features, including the head, shoulders, and hands are labeled manually to train a deep neural network model (Mathis et al., 2018), enabling feature extraction as described in the Methods section.

Resulting location scatterplots of head, shoulders, and hands are shown for two subjects in Fig. 2B and represent 8 hours of office work. Prior to data collection, participants are instructed to position the power caster and given a brief information on its function. A dummy wearable is placed on the right, proximal region of the arm of the participants. After collection, characteristics such as distance to the power caster and angular offset are subsequently computed (see Methods section). Resulting data for the cohort, shown in Fig. 2C and 2D, represent insight for localization parameters relevant for rectenna design. Fig. 2C shows the average of wearable to power casting system distance with a 95% confidence interval (shaded red). An average distance of 60.13 cm with a standard deviation of 20.30 cm is computed. This distribution is skewed towards shorter distance, showing a median value of 55.38 cm. Fig. 2D shows the average distribution of the orientation angle of the wearable to the power caster with an average of 54.09 degrees and a standard deviation of 26.73 degrees (confidence interval shaded blue).

For an office worker, a prolonged period of stationary behavior (86.4%) (Pollard et al., 2022) is recorded in literature. In our cohort, subject occupancy during the 8-hour experiments is defined as time spent within 150 cm of the transmitter. Fig. 2E demonstrates this feature extraction for one participant, with data indicating 7.12 hours spent within 150 cm of the transmitter, which accounts for 89.9% stationary time during the experiment. Across the cohort, an average of 72.68% of the day spent in the test location (standard deviation = 10.57%) and average occupancy time of 5.81 hours (standard deviation = 0.84 hours) is recorded (see Fig. 2F). Domain occupancy, when

paired with spatial location information, provides the fundamental framework for optimizing rectenna design for optimized energy harvesting.

A realistic estimation of power transfer to the device is shown in Fig. 2G for an ideal isotropic (0 dBi gain) antenna receiver as a function of distance to the power casting transmitter (see Methods section). The complex field behavior in the radiating near-field region of the transmitter cannot be adequately approximated using the classical Friis equation, which is only valid in the far-field. Therefore, the near-field power density distribution of a transmitter antenna with 3W EIRP and a similar size as the power caster is obtained from full-wave simulations (see Methods section). For the average distance of 60.13 cm obtained by the behavioral analysis, a power of 4.59 mW could be harvested as estimated under ideal conditions. To provide the best possible rectenna and wearable system design, the scenario specific information can be used to create hardware optimized to match the statistical average user. This is achieved through matching antenna, rectifier, load impedance, and spatial placement in the mesh based on angular statistics derived from behavioral data (see Fig. S1 and Fig. S2).

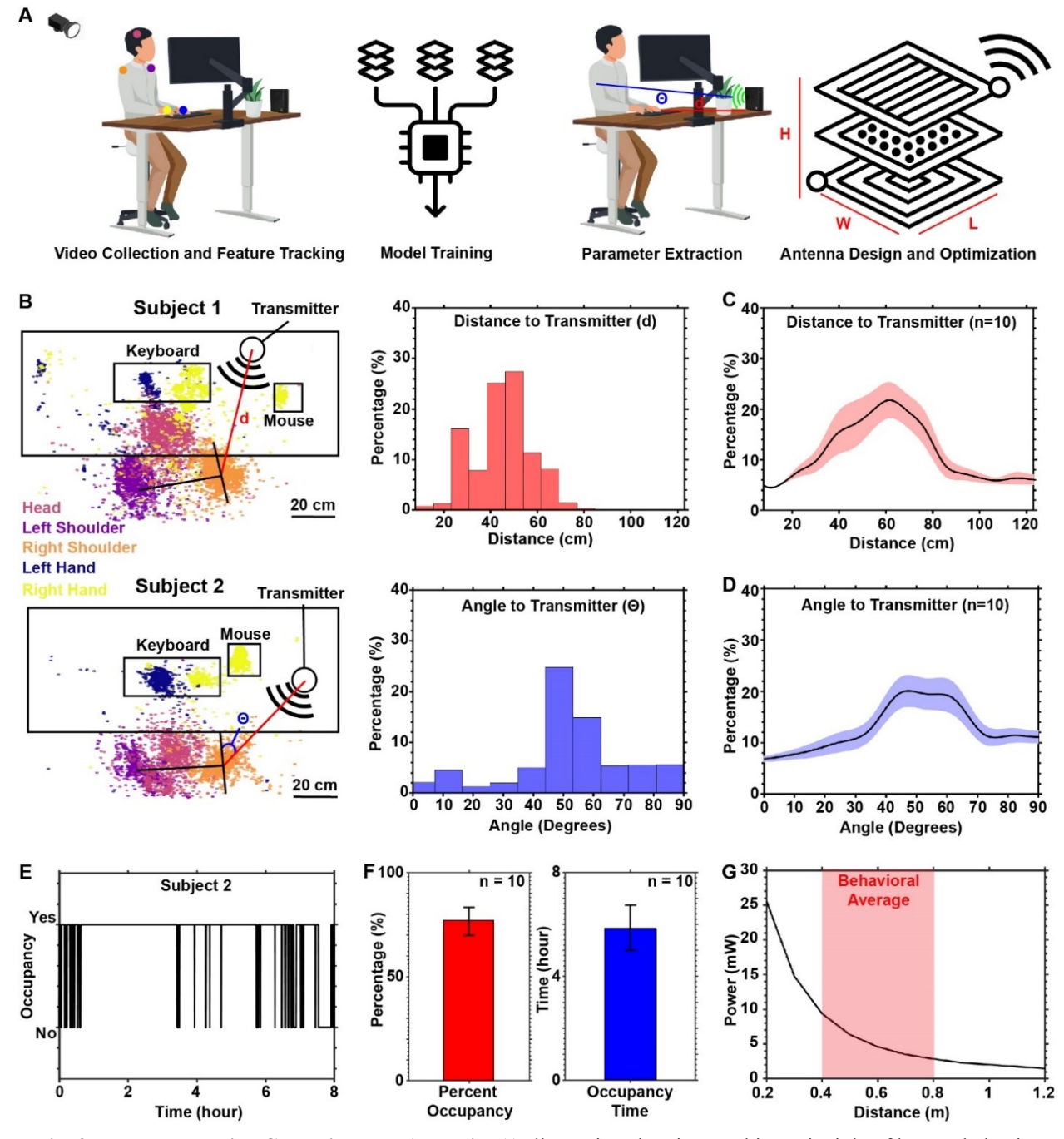


Fig. 2 Human Behavior Collection and Analysis: A) Illustration showing working principle of human behavior capture and analysis to drive antenna design. B) Parameter extraction from 2 participants showing heat mapped location of relevant physiological markers and subsequent distribution of key parameters, namely distance from the power caster (red) and angle offset from the power caster (blue). C) Distribution of distance from of the right shoulder to the power caster for individuals in an office setting (n=10) with 95% confidence interval (shaded red). **D)** Distribution of angle from of the right shoulder to the power caster for individuals in an office setting (n=10) with 95% confidence interval (shaded blue). **E)** Plot showing occupancy time of subject in the office space. **F)** Plots showing percentage of time during a workday occupying office space (red) and time spent in the office space (blue). **G)** Graph showing the maximum power received as a function of distance by an ideal isotropic antenna under power caster illumination (3W EIRP RF power), as obtained from full-wave electromagnetic simulations.

Context-aware Rectenna design

To make use of design considerations extracted from behavioral data, system level requirements for energy consumption, operational voltage and peak current requirements must also be considered. Fig. 3A shows an example of transient power requirements for a biosymbiotic wearable device that features a Bluetooth Low-Energy (BLE) system on a chip (SoC) and a variety of biosensors. Using increasing polling intervals for the sensors, power requirements can vary substantially, resulting in an average equivalent system load between 1-7 k Ω (see Fig 3A inset). Because devices include a small energy storage (either small battery or supercapacitor), average load is determined by sensor configuration and polling intervals for the biomedical application. Pairing this information with behavioral information, power casting systems can be optimized to deliver optimal power.

For the wearable configuration used in this work, a two-stage Dickson rectifier circuit is adopted (as shown in Fig. 3B) based on the operational parameters illustrated in Fig. 3A. To maximize WPT from the power caster to the rectifier circuit, complex conjugate matching is required between the antenna and the rectifier circuit. Input impedance of the rectifier circuit in its common operation modes (1 k Ω and 7 k Ω) is used to design the antenna. The input impedance of the rectifier circuit significantly depends on: 1) the available distance-dependent RF power level (shown in Fig. 2G), 2) the system load (shown in Fig. 3A), and 3) the diode specifications (BAT24-02LS, Infineon). The simulated input impedances of the rectifier circuit for the two extreme loading cases are compared in Fig. 3C, which shows real and imaginary part of the rectifier impedance as a function of distance from the transmitter. From 0 to 1.5 m the rectifier impedance changes steadily for both loads of 1 k Ω and 7 k Ω . The antenna can only be optimized to match a particular rectifier circuit input impedance; therefore, it is critical to select the impedance to be matched for power transfer efficiency over the distance range acquired from behavioral analysis.

To provide radiation patterns fitting the behavioral analysis, as well as to satisfy mechanical and wearability considerations, a planar antenna design is selected. Specifically, a planar inverted-F antenna (PIFA), which encompasses shorting pins, a feed point, and a dielectric insulating layer that separates the ground and a quarter-wave (shorted) resonant patch on the top surface. The device structure shown in Fig. 3D utilizes a digital design and manufacturing process (3D FDM printing) to achieve a customizable PIFA structure with flexible mechanics. The PIFA

structure is comprised of multiple layers of conductive and insulating dielectrics embedded into 3D printed thermoplastic polyurethane (TPU) ($\varepsilon_{TPU} = 3.3$, $\tan \delta = 0.09$, see Methods). The ground plane is comprised of a laser-structured copper-clad polyimide (Pyralux AG185018RY, Dupont) (details in the Methods section) and is spaced from the resonating plane with a 3D pillar structure designed to support the resonating plane with minimal dielectric loss while utilizing soft materials that can be structured into almost imperceptible designs. The laser-structured resonating plane is also encapsulated in a top layer of TPU to provide protection during everyday wear. Stretchable curvilinear 3D stretchable connections (C3Cs) link the resonant top patch and ground (Fig. 3D-E). A similar C3C structure is used to guide the feedline of the antenna into the rectifier circuit (Fig. 3E). Further details on material composition and device design can be found in Fig. S1.

Optimization of impedance and mechanics is accomplished with modulation of the serpentine mesh arc angle, defining the ground and radiation plane, and location of C3Cs (see Fig. S1). Combined with a matched rectifier, a maximum power point (MPP) tailored to operational distance and system load is accomplished. Two antennas are individually optimized for the representative rectifier input impedance values of 1 k Ω and 7 k Ω . The corresponding rectifier performance is shown in Fig. 3F, output voltage and power are simulated at a 50 cm distance from the power casting unit and displayed against system load matching the designed 1 and 7 k Ω (MPP) target. The 7 k Ω matched antenna design provides a higher output power over a broader range with an output of ~3.4 mW over a range of 5-10 k Ω system load, enabling flexibility in firmware design and current limitation for battery recharge schemes.

Based on behavioral analysis in Fig. 2C, operation at 40-80 cm from the power casting unit with an estimated system load of 7 k Ω is chosen for optimization. The resulting rectenna performance is shown in Fig. 3G-I, with further details in Fig. S3. Fig. 3G shows load sweep data for the rectenna at 0.5 m from the transmitter. The results measured in an anechoic chamber (Reference) environment achieve a good agreement with the corresponding results simulated in free space. It is important to note is that application performance can vary depending on environment through variation of casting angle, multipath effects (see Fig. S4) or shadowing from the human body (see Methods section). Fig. 3H shows power output of the device as a function of distance from the transmitter. Similarly, simulations offer a good prediction of performance in the anechoic environment, with performance discrepancies in the application scenario arising from the

use of commercially available power casting systems that feature higher gain transmission antennas (see Fig. S4). Fig. 3I shows rotational axis performance of the antenna structure in free space. Variations in performance about the yaw and pitch axis match simulated and recorded data, while corresponding data for the roll axis show discrepancies due to limitations on experimental set up. Results from these experiments show that design choices extracted from system level and behavioral information can be integrated into the digital design process to produce an antenna structure and orientation that can be carefully engineered in a simulated environment to yield rectennas that performs well over a broad range of application environments and scenarios (See Fig. S2 and Fig. S5). If application scenarios demand a larger angle of power harvesting, behavioral data can be consulted to design dual rectenna devices that enable bidirectional or nearly omnidirectional WPT with improved performance at the cost of increased system complexity and electronics footprint (See Fig. S2).

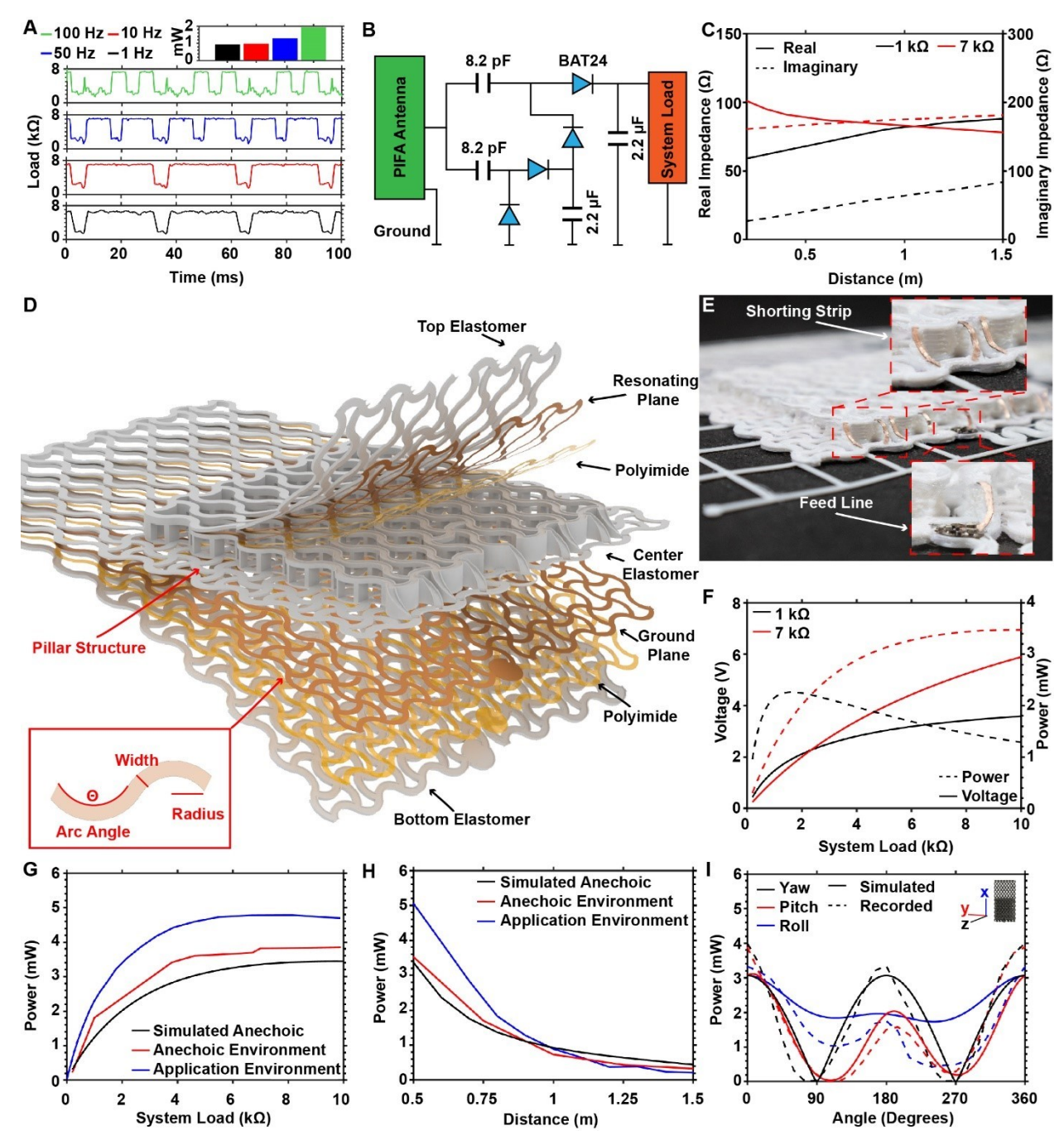


Fig. 3 Context-aware designed antenna performance: A) Plotting showing time-dependent system load with varying sampling rates. The bar graph shows the resulting average power consumption. B) Schematic showing Dickson circuit used for matching and rectification. C) Real and imaginary antenna impedances for two load values at increasing distances. D) Rendering showing constituent layers of the personalized on-body PIFA structure. E) Image showing 3D printed PIFA structure, highlighting ramps and shorting strips used to connect the resonating plane to the ground plane. F) Voltage and power curves of two antenna structures showing modulation of maximum power point of the system. G) Simulated and recorded values for load sweeps of the rectenna system at 0.5 m. H) Simulated and recorded voltage output as a function of distance from the transmitter for the 7 k Ω load design. I) Plot of simulated and recorded PIFA rectenna performance as a function of angular rotation along each x,y, and z axis in free space.

Mechanical Design and Fabrication

Integration of the 3D printed on-body antenna into a biosymbiotic wearable devices is carried out using design strategies and manufacturing schemes previously described in Stuart et al. (Stuart et al., 2021). The fabrication schemes enable tailoring of electromagnetics and mechanics for context-aware antenna design and allow for precise positioning of the antenna and personalized fit for the wearer, even on highly mobile regions of the body such as the shoulder (See Fig. S2 and Fig. S6) (Stuart et al., 2021). Important considerations are wearability and comfort that enables uninterrupted use over weeks. Fig. 4A details this process, where the personalized PIFA is integrated in biosymbiotic electronics using 3D data from scans of the user. Devices are manufactured using FDM printing with details presented in the Methods section and Fig. S7. Key to the realization of the on-body PIFA with relatively lossy TPU, which is incurred to enable mechanical structures that serve overall system performance goals, is the use of 3D printed pillar structures to support the resonating plane of the antenna above the ground plane (see Fig. 4B) with a minimum amount of material. Modulation of pillar density, as seen in Fig. S8, enables complex features that would not be obtainable with conventional fabrication techniques.

The structural makeup of the pillar drives both mechanical and electromagnetic performance of the antenna, with tradeoffs between mechanical stiffness and effective permittivity of the insulating layer. Fig. 4C shows results simulated at 915 MHz for the effective relative permittivity of the layer separating radiation and ground plane with increasing pillar density. As the amount of material decreases, the effective permittivity and correspondingly the effective dielectric constant loss decrease. Therefore, from the point of view of electromagnetic radiation, lower pillar density is preferred because of lower dielectric loss; however, limitations of the fabrication process result in a 10% pillar density limit required for structural integrity. Additionally, mechanical considerations for practical applications limit stiffness and therefore pillar density due to external forces such as compression from clothing, that can cause variation in antenna performance (see Fig. S9). Fig. 4D shows the force required for structural deformation of the antenna with 15, 25, and 50% pillar density over increasing applied force (see Methods section). Pillar collapse occurs with as little as 5N, which in turn detunes the antenna resulting in reduced power output. For our design a pillar density 16% was used, which together with the PIFA

antenna is electromagnetically robust and presents a good compromise between antenna performance and robustness in real life scenarios.

254

255

256

257

258

259

260

261

262

263

264

265

266

267

268

269

270

271

In addition to antenna compression, lateral deformation in integrated mesh structures must also be considered in the design and implementation of the final device. Fig. 4E shows finiteelement-analysis (FEA) of a mesh structure with embedded PIFA oriented along the X axis (results with the PIFA oriented in the Y axis can be found in Fig. S10). In the FEA models, system strain, which is applied to the mesh housing the antenna, is primarily distributed within peripheral linear structure, which yields minor deformation in the antenna structure when strained to 30% displacement. It is important to note limitations of the analysis with large deformation of elastomeric material that result in edge effects seen in Fig. S10, which may not be present in an integration in a wearable. In either orientation, the placement of the antenna structure demonstrates minimal effect on the mechanical properties of the system (as shown in Fig. S10). Minor deformations in the ground plane result in minimal effect on electromagnetic properties, as shown in Fig. 4F. In the most extreme case, power output of the antenna is reduced by 2.3%. The scenarios covered in this figure demonstrate the worst-case scenario for wearable applications such as placement on highly mobile locations such as the elbow (30% strain) (Sun et al., 2018; Stuart et al., 2021). During normal daily activity, the strain experienced by the device has no measurable impact on the performance of the system, as detailed in cyclic strain tests (100k cycles) Fig. S11.

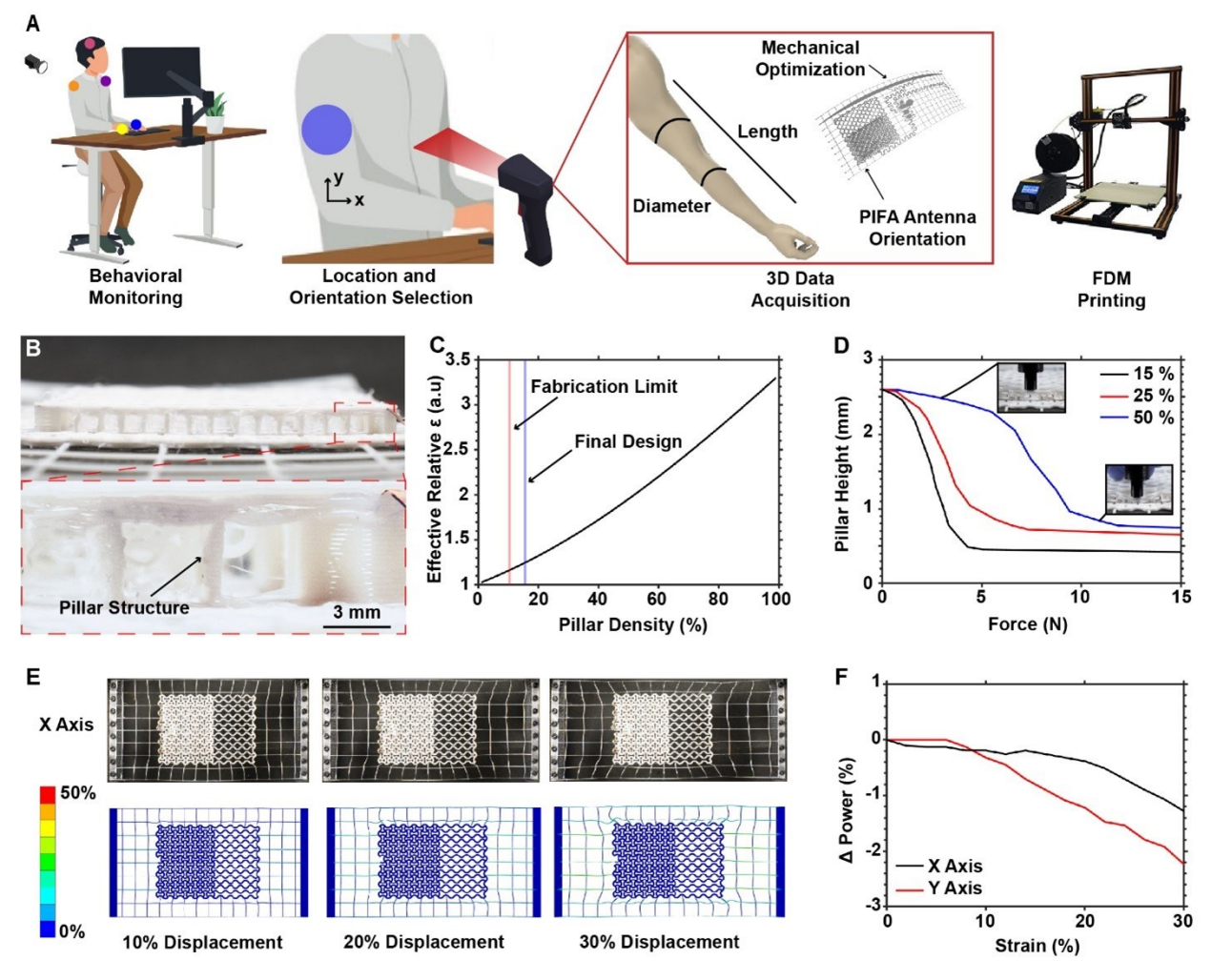


Fig. 4 Mechanical Considerations for Personalized Antenna Structures: A) Illustration showing mechanical design process that utilizes behavioral analysis and digital design to form location and mechanical optimization of personalized biosymbiotic devices. **B)** Photo of 3D printed pillar structure used to support the resonating plane from the ground plane. **C)** Plot of effective permittivity of the insulating layers as a function of 3D printed pillar density. **D)** Plot of compression force needed to collapse pillar structure with varying pillar density. **E)** FEA of PIFA embedded into mesh design in a horizontal orientation. **F)** Change in power as a function of strain applied on the system for PIFA embedded in various orientations.

Long-term Data Acquisition Without User Interaction

With concepts introduced here, significant power transfer to the wearable is expected, enabling continuous operation and multimodal high-fidelity recording of biosignals. To demonstrate this capability, a system with BLE SoC, multimodal sensors, context-aware antenna designs, and soft mechanics is created (see Fig. S1). Fig. 5A-B shows device composition, simplified electrical schematic, image of the device located on the proximal region of the upper arm, and images of sensing nodes with corresponding characteristic performance graphs. The

device features the PIFA and associated rectifiers introduced in Fig. 3. Power from the rectification circuit is sent to a power management IC, which includes maximum power point tracking (MPPT) control. A small (9 mm x 9 mm) battery (25 mAh) is used to provide power to the device during operation outside of the power casting area. A BLE SoC controls peripheral sensors and relays collected data via a 2.45 GHz antenna (see methods section). This device hosts multimodal sensing capabilities including a sub millikelyin resolution temperature sensor, a 3D-printed circumferential strain gauge, and a relative humidity sensor. Each sensor utilizes commercially available components integrated on rigid islands of no more than 6 mm in diameter to enable system level soft mechanics (Stuart et al., 2021), and is connected using serpentine interconnects placed at physiologically relevant locations extracted from the 3D data as detailed in Fig. 4A. Sensor performance, which benefits from conformal and circumferential attachment to the body is characterized with simple experiments analog to our previous work (Stuart et al., 2021). In the graphs shown in Fig. S12-S14, red shaded area shows biceps contraction, exercise induced temperature and humidity changes with characteristic performance of muscle strain sensors $(7.14 \times 10^{-4} \, \% \, \text{Strain}/\Omega)$, thermography sensors (2.12 K/V) and skin humidity (33.9 $\% \, \text{RH/V}$). The sensors show robust operation and the ability to detect small changes in physiological signals independent of changes to ambient conditions (see Fig. S15)

To demonstrate long-term, uninterrupted operation capabilities of the device a 14-day experiment is performed. The device was deployed on the proximal region of the bicep for imperceptible use with several types of daily outfits including summer wear such as tank tops and t-shirts, as well as winter wear such as thick jackets and sweatshirts that showed a negligible effect (\pm 4%) on WPT efficiency (see Fig. S16). No effects on the underlying epidermis, such as irritation, are observed (see Fig. S17). Data is summarized in Fig. 5C showing continuously captured raw data over 2 weeks. During the test, the device is only recharged when in proximity of a power caster located at the work location on the desk, as outlined in the behavioral analysis section. Battery voltage is monitored at regular intervals, with regions shaded in green indicating proximity to a power casting unit. Recorded battery voltage never falls below 3.49 V during the experiment, demonstrating robust operation without reliance on human interaction for recharging. Operation

308

309

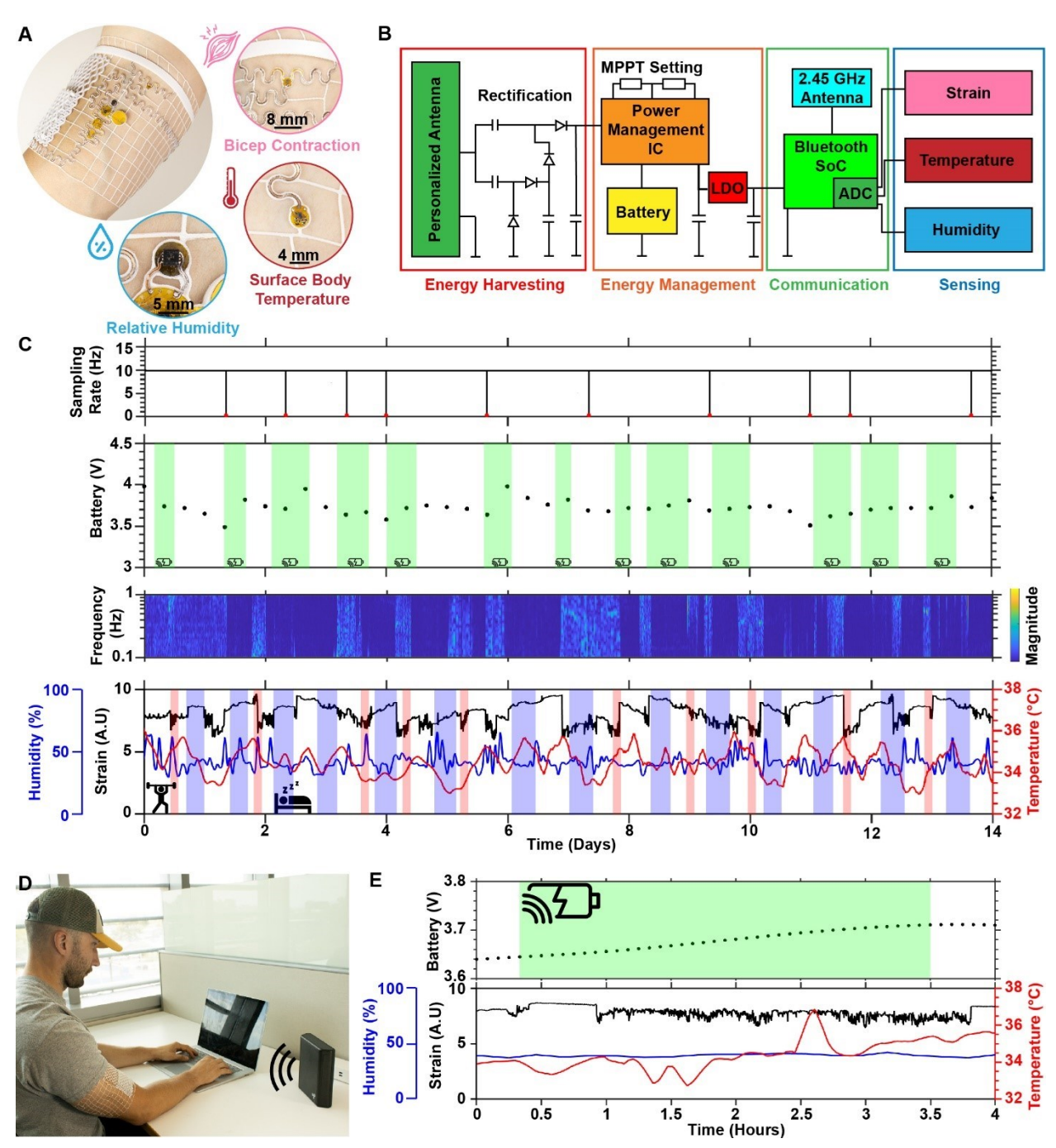


Fig. 5 Long-term System Demonstration and Performance: A) Image showing biosymbiotic device used for long-term collection of biodata with sensors highlighted. B) Simplified electronic circuit schematic showing composition of biosymbiotic device. C) Data collected from 14-day experiment showing collection of sampling rate (top graph), battery voltage (middle graph), temperature (red), humidity (blue), strain (black), and corresponding continuous wavelet transform. D) Image of device operation in an office setting. E) Plot of 4 hours of data collected during office occupancy, showing passive battery recharge over time with continuously collection of temperature, humidity, and strain.

primarily occurs during periods of sleep or intense daily activity, with a mean dropout time of 79.5 seconds and a median time of 49 seconds (See Fig. S18). The total sample time lost is 15 minutes, equating to a loss of 0.06% of total data during the experimental period. Strain data is visualized in the frequency domain using a continuous wavelet transform to show periods of increased bicep contraction frequency, matching periods of physical exercise (shaded red). Similarly, incidences of increased activity overlap with increases in humidity, showing the capability to monitor perspiration. Device usage in a typical office setting is shown in Fig. 5D with transmitter located approximately 50 cm from the device. The corresponding data shown in Fig. 5E highlights a charging period where battery voltage is increased by 100 mV in ~ 3h at the desk corresponding to a charge rate of 2.2 mW (average system power consumption of 2.15 mW, resulting in 4.35 mW of average power transfer to the wearable). Fig. S19 shows device operation in a gym setting with the subject performing a bicep curl. Corresponding data also displayed in Fig. S19, which shows 2 hours of data before, during, and after the training session, demonstrating the capability to record high-fidelity biosignals in highly air-conditioned environments with high amount of air movement. In this graph, a steady increase in body temperature is observed during the period of activity, correlating with an increase in localized humidity. Additionally, continuous activity of bicep strain is observed (6 contractions/min), with periods of increased frequency (50 contractions/min) denoting exercises that specifically target that muscle group.

Conclusion

310

311

312

313

314

315

316

317

318

319

320

321

322

323

324

325

326

327

328

329

330

331

332

333

334

335

336

337

338

339

Development of wearable devices intended for continuous recording on the body such as digital medicine applications still grapple with user acceptance and face many technological hurdles that impede performance, impacting their use as diagnostic and therapeutic tools. One of the most challenging aspects is user retention of wearable devices, which only have an average use time of 12 months (Lazar et al., 2015; Ledger and McCaffrey, 2014; Maher et al., 2017; Stuart et al., 2022). Imperceptible devices that eliminate recharging and interaction requirements with wearable technologies are core to advance digital medicine applications.

Accomplishing advances electromagnetically and mechanically is highly complex because performance gains in one area likely impact others. Critical is balanced system level performance to enable operation over weeks and months without impacting daily activities. The framework introduced here using behavioral analysis and digital manufacturing techniques to enable context-

aware antenna and rectifier designs to optimize power transfer with an on-body antenna to enable indefinite device operation. The resulting system level insight provides a performance envelope that takes electromagnetic, mechanical, and sensing performance into account to deliver a balanced data-driven design approach with context-aware solutions to enable indefinitely operating wearables.

Deployment of these design strategies for on-body antennas also introduces a methodology to assist in development of antennas, rectifiers and systems for wireless devices that is transferrable to contexts other than wearables and applies to many scenarios that involve technologies used in proximity or by human subjects. For example, context-aware designs can aid WPT design for human interfaces such as wireless mice, keyboards, game controllers, headphones etc. and other wearables such as wrist mounted fitness devices.

Acknowledgments

Funding

T.S. and P.G. acknowledge support from the Flinn Foundation Translational Bioscience Seed Grant Pilot Program. T.S. and P.G. acknowledge support from the National Science Foundation I-Corp program. T.S. acknowledges support from the Provost's Investment Fund at the University of Arizona. P.G acknowledges the Arizona SensorLab Student and Seed Grant.

Author contributions

T.S., X.Y., S.J.C., C.F., P.G. conceptualized the project. T.S. contributed to design of video capture hardware, data processing and analysis of behavioral data, fabrication of rectennas, collection of and analysis of mechanical data, FEA simulations, fabrication of biosymbiotic devices, characterization of sensors, collection of rectenna data in application settings, collection and interpretation of long-term data collection, and image collection. X.Y. contributed to rectifier circuit design, electromagnetic characterization of material, electromagnetic simulations, antenna design, experimental characterization of the rectenna in anechoic environment and processing of rectenna measurement data. M.F. contributed to design of video capture hardware, fabrication of rectennas, fabrication of biosymbiotic devices, collection of rectenna data in application settings, FEA simulation, characterization of sensors, and image collection. D.T.M. contributed to fabrication of rectennas, collection of rectenna data in application settings, and image collection. N.R. contributed to collection of rectenna data in application settings and image collection. S.D.

- 371 contributed to collection of mechanical compression data and image collection. S.J.C. and C.F.
- provided supervision and contributions to the antenna and rectifier concepts and interpretation of
- 373 the results. P.G. provided supervision and contributions to the antenna and rectifier concepts,
- supervision and contributions to behavioral data collection and analysis, supervision and
- 375 contributions to mechanical simulation results, supervision and contributions to long-term data
- 376 collection and analysis. All authors contributed to review and revision of the manuscript.

377 Competing Interests

378 Authors declare that they have no competing interests.

379 Data and Materials Availability

All data needed to evaluate the conclusions in the paper are present in the paper and/or

381 the Supplementary Materials.

382

383

References

- Rogers, J.A., Takao, S., Yonggang, H., 2010. Materials and Mechanics for Stretchable
- 385 Electronics. Science 327, 1603–1607.
- Cho, S., Ensari, I., Weng, C., Kahn, M.G., Natarajan, K., 2021. Factors affecting the quality of
- person-generated wearable device data and associated challenges: Rapid systematic review.
- JMIR Mhealth Uhealth 9, e20738.
- Choi, Y.-M., Lee, M.G., Jeon, Y., 2017. Wearable biomechanical energy harvesting
- technologies. Energies (Basel) 10, 1483.
- Dang, Q.H., Chen, S.J., Ranasinghe, D.C., Fumeaux, C., 2020. Modular Integration of a Passive
- 392 RFID Sensor With Wearable Textile Antennas for Patient Monitoring. IEEE Trans Compon
- Packaging Manuf Technol 10, 1979–1988.
- Dobkin, D.M., 2012. The rf in RFID: uhf RFID in practice. Newnes.
- Eid, A.M., Alieldin, A., El-Akhdar, A.M., El-Agamy, A.F., Saad, W.M., Salama, A.A., 2021. A
- novel high power frequency beam-steering antenna array for long-range wireless power
- transfer. Alexandria Engineering Journal 60, 2707–2714.
- Elleuch, R., Elleuch, K., Salah, B., Zahouani, H., 2007. Tribological behavior of thermoplastic
- polyurethane elastomers. Mater Des 28, 824–830.
- 400 Fensli, R., Pedersen, P.E., Gundersen, T., Hejlesen, O., 2008. Sensor acceptance model-
- measuring patient acceptance of wearable sensors. Methods Inf Med 47, 89–95.
- Heikenfeld, J., Jajack, A., Rogers, J., Gutruf, P., Tian, L., Pan, T., Li, R., Khine, M., Kim, J.,
- Wang, J., Kim, J., 2018. Wearable sensors: modalities, challenges, and prospects. Lab Chip
- 404 18, 217–248.

- 405 Huang, X., Liu, Y., Kong, G.W., Seo, J.H., Ma, Y., Jang, K.-I., Fan, J.A., Mao, S., Chen, Q., Li,
- D., others, 2016. Epidermal radio frequency electronics for wireless power transfer.
- 407 Microsyst Nanoeng 2, 16052.
- Insafutdinov, E., Pishchulin, L., Andres, B., Andriluka, M., & Schiele, B. (2016, October).
- Deepercut: A deeper, stronger, and faster multi-person pose estimation model. In European
- conference on computer vision (pp. 34-50). Springer, Cham.
- Kekade, S., Hseieh, C.-H., Islam, Md.M., Atique, S., Mohammed Khalfan, A., Li, Y.-C., Abdul,
- S.S., 2018. The usefulness and actual use of wearable devices among the elderly population.
- 413 Comput Methods Programs Biomed 153, 137–159.
- 414 Kim, J., Banks, A., Xie, Z., Heo, S.Y., Gutruf, P., Lee, J.W., Xu, S., Jang, K.-I., Liu, F., Brown,
- G., Choi, J., Kim, J.H., Feng, X., Huang, Y., Paik, U., Rogers, J.A., 2015. Miniaturized
- Flexible Electronic Systems with Wireless Power and Near-Field Communication
- 417 Capabilities. Adv Funct Mater 25, 4761–4767.
- Kim, J., Gutruf, P., Chiarelli, A.M., Heo, S.Y., Cho, K., Xie, Z., Banks, A., Han, S., Jang, K.-I.,
- Lee, J.W., Lee, K.-T., Feng, X., Huang, Y., Fabiani, M., Gratton, G., Paik, U., Rogers, J.A.,
- 420 2017. Miniaturized Battery-Free Wireless Systems for Wearable Pulse Oximetry. Adv
- 421 Funct Mater 27, 1604373.
- Krishnan, S.R., Su, C.-J., Xie, Z., Patel, M., Madhvapathy, S.R., Xu, Y., Freudman, J., Ng, B.,
- Heo, S.Y., Wang, H., others, 2018. Wireless, Battery-Free Epidermal Electronics for
- 424 Continuous, Quantitative, Multimodal Thermal Characterization of Skin. Small 14,
- 425 1803192.
- Lazar, A., Koehler, C., Tanenbaum, T.J., Nguyen, D.H., 2015. Why we use and abandon smart
- devices, in: Proceedings of the 2015 ACM International Joint Conference on Pervasive and
- 428 Ubiquitous Computing. pp. 635–646.
- Ledger, D., McCaffrey, D., 2014. Inside wearables: How the science of human behavior change
- offers the secret to long-term engagement. Endeavour Partners 200, 1.
- Lee, K., Kim, J., Cha, C., 2019. Microwave-based wireless power transfer using beam scanning
- for wireless sensors, in: IEEE EUROCON 2019-18th International Conference on Smart
- 433 Technologies. IEEE, pp. 1–5.
- Lim, H., Kim, H.S., Qazi, R., Kwon, Y., Jeong, J., Yeo, W., 2020. Advanced soft materials,
- sensor integrations, and applications of wearable flexible hybrid electronics in healthcare,
- energy, and environment. Advanced Materials 32, 1901924.
- Maher, C., Ryan, J., Ambrosi, C., Edney, S., 2017. Users' experiences of wearable activity
- trackers: a cross-sectional study. BMC Public Health 17, 1–8.
- Mathis, A., Mamidanna, P., Cury, K.M., Abe, T., Murthy, V.N., Mathis, M.W., Bethge, M.,
- 2018. DeepLabCut: markerless pose estimation of user-defined body parts with deep
- 441 learning. Nat Neurosci 21, 1281–1289.

- Mercer, K., Giangregorio, L., Schneider, E., Chilana, P., Li, M., Grindrod, K., 2016. Acceptance
- of Commercially Available Wearable Activity Trackers Among Adults Aged Over 50 and
- With Chronic Illness: A Mixed-Methods Evaluation. JMIR Mhealth Uhealth 4, e7.
- Nath, T., Mathis, A., Chen, A.C., Patel, A., Bethge, M., Mathis, M.W., 2019. Using DeepLabCut for 3D markerless pose estimation across species and behaviors. Nat Protoc 14, 2152–2176.
- Nozariasbmarz, A., Collins, H., Dsouza, K., Polash, M.H., Hosseini, M., Hyland, M., Liu, J.,
- Malhotra, A., Ortiz, F.M., Mohaddes, F., 2020. Review of wearable thermoelectric energy
- harvesting: From body temperature to electronic systems. Appl Energy 258, 114069.
- 450 Pollard, B., McDonald, G., Held, F., Engelen, L., 2022. Stop motion: using high resolution
- spatiotemporal data to estimate and locate stationary and movement behaviour in an office
- workplace. Ergonomics 65, 675–690.
- Rahman, M.A., Cai, L., Tawfik, S.A., Tucker, S., Burton, A., Perera, G., Spencer, M.J.S., Walia,
- S., Sriram, S., Gutruf, P., Bhaskaran, M., 2022. Nicotine Sensors for Wearable Battery-Free
- 455 Monitoring of Vaping. ACS Sens 7, 82–88.
- Ray, T., Choi, J., Reeder, J., Lee, S.P., Aranyosi, A.J., Ghaffari, R., Rogers, J.A., 2019. Soft,
- skin-interfaced wearable systems for sports science and analytics. Curr Opin Biomed Eng 9,
- 458 47–56.
- Ray, T.R., Choi, J., Bandodkar, A.J., Krishnan, S., Gutruf, P., Tian, L., Ghaffari, R., Rogers,
- J.A., 2019. Bio-Integrated Wearable Systems: A Comprehensive Review. Chem Rev.
- Shadid, R., Noghanian, S., 2018. A literature survey on wireless power transfer for biomedical
- devices. Int J Antennas Propag 2018.
- Shuai, K., Yang, J., Liu, C., Yang, X., Liu, X., 2021. Beam-steering transmitarray with active
- 464 frequency selective surface for wireless power transmission. International Journal of RF and
- 465 Microwave Computer-Aided Engineering 31, e22907.
- Spagnolli, A., Guardigli, E., Orso, V., Varotto, A., Gamberini, L., 2015. Measuring user
- acceptance of wearable symbiotic devices: validation study across application scenarios, in:
- International Workshop on Symbiotic Interaction. Springer, pp. 87–98.
- Stuart, T., Cai, L., Burton, A., Gutruf, P., 2021. Wireless and battery-free platforms for
- collection of biosignals. Biosens Bioelectron 178, 113007.
- Stuart, T., Hanna, J., Gutruf, P., 2022. Wearable devices for continuous monitoring of biosignals:
- 472 Challenges and opportunities. APL Bioeng 6, 021502.
- Sun, C., Cheng, J., Ohira, T., 2008. Handbook on advancements in smart antenna technologies
- for wireless networks. IGI Global.
- Sun, J., Zhao, Y., Yang, Z., Shen, J., Cabrera, E., Lertola, M.J., Yang, W., Zhang, D., Benatar,
- A., Castro, J.M., 2018. Highly stretchable and ultrathin nanopaper composites for epidermal
- strain sensors. Nanotechnology 29, 355304.

- Sunwoo, S.-H., Ha, K.-H., Lee, S., Lu, N., Kim, D.-H., 2021. Wearable and implantable soft
- bioelectronics: Device designs and material strategies. Annu Rev Chem Biomol Eng 12,
- 480 359–391.
- Tong, H., Geyi, W., 2016. Optimal design of smart antenna systems for handheld devices. IET Microwaves, Antennas & Propagation 10, 617–623.
- Stuart, T., Kasper, K. A., Iwerunmor, I. C., McGuire, D. T., Peralta, R., Hanna, J., Johnson, M.,
- Farley, M., LaMantia, T., Udorvich, P., Gutruf, P., 2021. Biosymbiotic, personalized, and
- digitally manufactured wireless devices for indefinite collection of high-fidelity biosignals.
- 486 Sci Adv 7, eabj3269.
- Wei, K., Kording, K.P., 2018. Behavioral tracking gets real. Nat Neurosci 21, 1146–1147.
- Willis, C. M., Shaw, S., De Lacharriere, O., Baverel, M., Reiche, L., Jourdain, R., ... &
- Wilkinson, J. D. (2001). Sensitive skin: an epidemiological study. British Journal of
- 490 Dermatology, 145(2), 258-263.
- 491 Xia, M., Aissa, S., 2015. On the efficiency of far-field wireless power transfer. IEEE transactions 492 on signal processing 63, 2835–2847.
- Xu, C., Song, Y., Han, M., Zhang, H., 2021. Portable and wearable self-powered systems based on emerging energy harvesting technology. Microsyst Nanoeng 7, 1–14.
- Yang, C., Vora, H.D., Chang, Y., 2018. Behavior of auxetic structures under compression and impact forces. Smart Mater Struct 27.
- 497 Yedavalli, P.S., Riihonen, T., Wang, X., Rabaey, J.M., 2017. Far-field RF wireless power
- transfer with blind adaptive beamforming for Internet of Things devices. IEEE Access 5,
- 499 1743–1752.

508

- Yin, Z., Yan, J., Fang, S., Wang, D., Han, D., 2022. User acceptance of wearable intelligent
- medical devices through a modified unified theory of acceptance and use of technology.
- Ann Transl Med 10.
- Yu, X., Xie, Z., Yu, Y., Lee, J., Vazquez-Guardado, A., Luan, H., Ruban, J., Ning, X., Akhtar,
- A., Li, D., others, 2019. Skin-integrated wireless haptic interfaces for virtual and augmented
- reality. Nature 575, 473–479.
- Zou, Y., Bo, L., Li, Z., 2021. Recent progress in human body energy harvesting for smart
- bioelectronic system. Fundamental Research 1, 364–382.